Optimisation of Artefact Removal Algorithm for Microwave Imaging of the Axillary Region Using Experimental Prototype Signals

Daniela M. Godinho*, João M. Felício†, Carlos A. Fernandes‡, Raquel C. Conceição*
*Instituto de Biofísica e Engenharia Biomédica, Faculdade de Ciências da Universidade de Lisboa, 1749-016 Lisbon, Portugal, dgodinho94@gmail.com
†Centro de Investigação Naval (CINAV), Escola Naval, Almada, Portugal
‡Instituto de Telecomunicações, Instituto Superior Técnico, Universidade de Lisboa, Lisbon, Portugal

***Abstract*—Microwave Imaging (MWI) has the potential to aid breast cancer staging through the detection of Axillary Lymph Nodes (ALNs). This type of system can present some challenges, mainly due to the irregular axillary surface. The optimisation of the artefact removal algorithm to successfully remove the surface reflections is of great importance. In this paper, we propose using Singular Value Decomposition (SVD) as an artefact removal algorithm and study the effect of choosing different subsets of antenna positions for artefact removal on imaging results using experimental signals. We show that different subsets of antenna positions affect the results and in some cases prevent the targets detection. Our analysis allowed us to find an optimal combination of parameters which results in Signal-to-Clutter Ratio higher than 2.77 dB and Location Error lower than 14.9 mm for three different experimental tests. These results are relevant for the development of dedicated algorithms for ALN-MWI application.**

***Index Terms*—artefact removal algorithm, axillary lymph nodes, breast cancer, microwave imaging.**

I. Introduction

Breast cancer can metastasise to surrounding lymph nodes, specifically Axillary Lymph Nodes (ALNs). The number of metastasised lymph nodes is one of the indicators used for breast cancer staging and its assessment is important to determine treatment approaches [1]. Current pre-surgical and non-invasive medical imaging techniques still lack high sensitivity and specificity [2]. The most accurate technique to confirm ALN diagnosis is Sentinel Lymph Node Biopsy (SLNB), which is a surgical procedure where the first lymph node receiving drainage from the tumour is removed and sent to pathological analysis. Thus, there is a need for additional non-invasive and low-cost techniques to diagnose ALNs.

Our group has been working on a Microwave Imaging (MWI) system to detect and diagnose ALNs [3], [4], [5]. MWI is a low-cost and low-power technique and has had promising results for early breast cancer diagnosis [6] and brain stroke detection [7]. ALN-MWI presents several challenges compared to other well-studied applications (i.e. breast and head), namely: the axillary region has an irregular shape which hampers the performance of artefact removal algorithms; the use of a coupling medium to minimise skin reflections is not practical due to the morphology and size of the axillary region; and the torso limits the scan range of the antenna. One way to address these challenges is to find an optimal artefact removal procedure which can reduce the effects of the irregularity of the axillary region shape on the algorithms performance. In this paper, we study the performance of the artefact removal algorithm with different antenna positions and different algorithm parameters on our world-first experimental MWI prototype designed to image the axillary region.

II. Experimental prototype system

The prototype works as a monostatic system, with a single antenna scanning a 3D-printed anthropomorphic phantom of the axillary region (Fig. 1). The phantom was segmented from a Computed Tomography (CT) image [8] and then we 3D-printed the outer shape of the body using Polylactic Acid (PLA) [9]. The antenna is a Vivaldi antenna operating in air without body contact, impedance-matched in the $2-7$ GHz frequency band [10]. The phantom is positioned as a patient would in a clinical scenario, lying sideways on one of the arms extended along the head. An ALN model was embedded in the body phantom with the help of a plastic support, as shown in Fig. 1(c-d). The ALN was 3D-printed with the following approximate dimensions $20 \times 13 \times 11$ mm^3. Both the cavities of the axillary region and ALN models were filled with liquid mixtures [11] mimicking fat and metastasised ALN tissues, respectively. The information about the dielectric properties of metastasised ALNs is still limited [4], [5], [12], [13], so we assumed they have similar dielectric properties to breast tumours.

A. Antenna positioning

The antenna is swept in a cylindrical configuration around the phantom. For the present anthropomorphic phantom, a total of 72 antenna positions were considered. These positions are distributed in 9 angular positions (A to I) with 10° angular steps, and 8 horizontal antenna positions (1 to 8) with 10 mm steps, as shown in the measurement grid ($\mathbf{G_M}$) in Fig. 2.

Four anatomical references were considered to define the limits of the measurement grid ($\mathbf{G_M}$): the first angular position

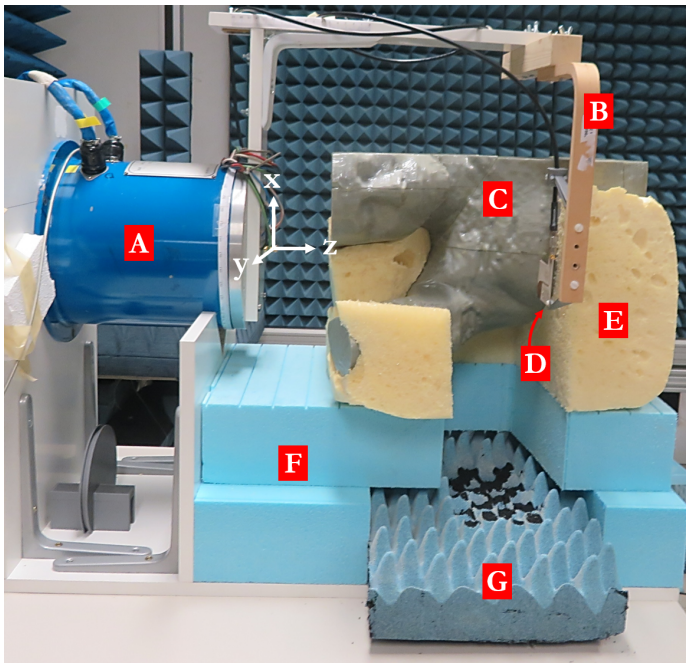

(a)

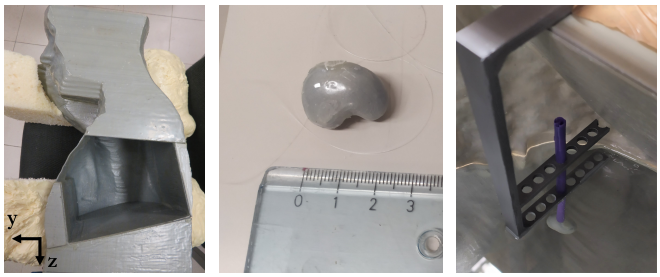

(b) (c) (d)

Fig. 1. Measurement setup and phantoms. (a) shows the setup with all components (roll positioner [A], antenna support arm [B], phantom [C], the antenna [D], styrofoam supporting the phantom [E, F] and electromagnetic absorber [G]). The white coordinate system represents the rotation and translation movements of the arm and antenna. The cavity of the axillary phantom is shown in (b), the axillary lymph node phantom in (c) and the support to place the lymph node within the phantom in (d).

(A) considers the sagittal plane (x-plane) through the nipple; the last angular position (I) considers the mid-coronal plane (y-plane which divides the body in half); the first horizontal position (1) considers the axial plane (x-plane) of the clavicle; and the last horizontal position (8) considers the axial plane of the nipple. These reference points can result in a $\mathbf{G_M}$ of variable size for different patients, covering different volumes and maintaining the spacing between antennas. Also, the volume of interest where the lymph nodes are located is expected to vary from patient to patient.

The optimal subset of antenna positions used for image reconstruction is denominated $\mathbf{G_I}$. The radial distance between each antenna position and the phantom surface ranges from 4 to 56 mm, with an average of 35 mm. The distances are represented in Fig. 3.

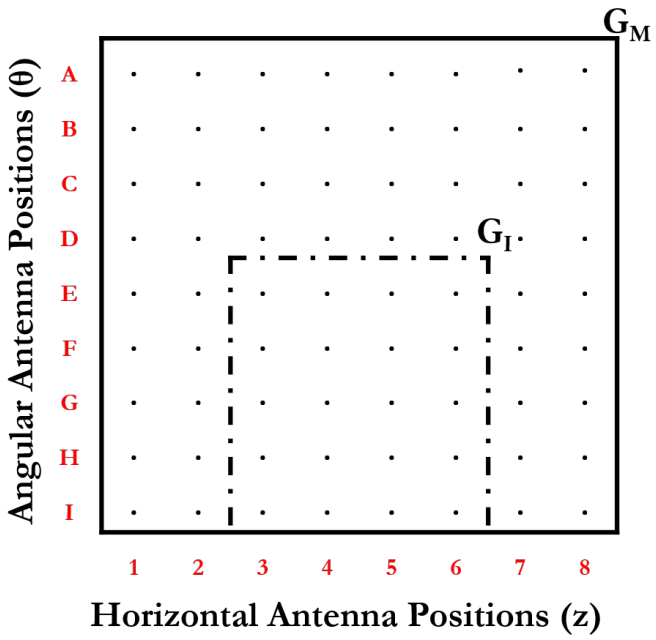

Fig. 2. Flattened view of cylindrical antenna position grid. $\mathbf{G_M}$ (delimited by solid line) designates the set of all points of the measurement grid, and $\mathbf{G_I}$ (delimited by dash-dot line) represents the subset of antenna positions used for image reconstruction.

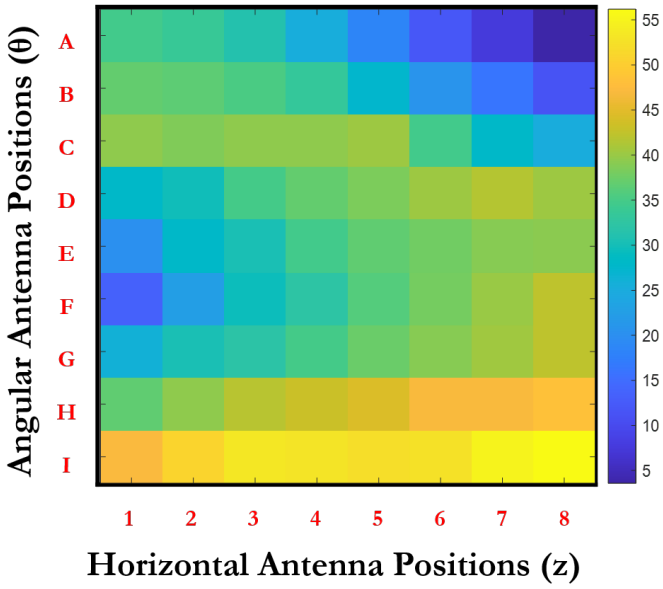

Fig. 3. Radial distance (in millimeter) between each antenna position and the phantom surface represented in a flattened view of cylindrical antenna position grid.

III. Signal Processing Algorithms

In this section, we present the artefact removal algorithm and the corresponding parameters. We then present the imaging algorithm and the performance metrics we use to evaluate the resulting images and the performance of the artefact removal

algorithm.

A. Artefact Removal Algorithm

The air/dielectric reflections are removed with a Singular Value Decomposition (SVD) algorithm [14]. SVD factorises a matrix of $m \times n$ into $\min[m; n]$ singular vectors and values, as presented in [14]. In our study, each column of matrix $\mathbf{M}$ corresponds to the input reflection coefficient $\mathbf{s}_{a,h}$, which results from the difference between the measured input reflection coefficient in the presence of the phantom and the measured coefficient in free-space. The indices a and h correspond to the indices of each angular and horizontal antenna positions, respectively. The number of columns n of matrix $\mathbf{M}$ corresponds to the number of input reflection coefficients considered for the factorisation and the number of rows m corresponds to the number of frequency points of each input reflection coefficient.

The first singular vectors obtained from SVD represent the highest magnitude reflections common to all signals of matrix $\mathbf{M}$. Hence, the air/dielectric response may be removed with SVD if it is similar between all signals of matrix $\mathbf{M}$. We emphasise that this kind of artefact removal relies very much on the similarity between signals, which is greatly affected by the antenna-phantom surface distance. Therefore, there is a need to perform this study in order to discover which subsets of antenna positions are the most reliable and provide the most accurate results.

In order to address the wide range of distances from each antenna position to the phantom, for each antenna position (a, h), SVD is applied to a matrix including the signal $\mathbf{s}_{a,h}$ and the neighbouring antenna positions' signals. The signals without the air/dielectric response ($\mathbf{M}^{cal}$) are obtained by subtracting the contribution from the first singular vectors from $\mathbf{M}$. The optimal number of singular vectors to remove needs to be determined since more than one singular vector can contain the air/dielectric response due to the irregular shape of the axillary region and one needs to ensure the ALN response is not present in the removed singular vectors.

The optimal removal of the air/dielectric response can be obtained by finding the combination of the subset of neighbouring antenna positions and the number of singular vectors removed which results in a successful target detection with the best imaging performance metrics. In this study, we test different subsets of neighbouring antenna positions with different patterns, as shown in Fig. 4. The subsets include 3 to 9 antenna positions and are named accordingly to their shape and number of antenna positions: Vertical 3 (Fig. 4a), Horizontal 3 (Fig. 4b), Diagonal 3 (Fig. 4c), Cross 5 (Fig. 4d), Diagonal 5 (Fig. 4e) and Block 9 (Fig. 4f). A range of different number of singular vectors are removed. For each subset, this number is limited by the number of signals of matrix $\mathbf{M}$, for example if the number of signals (i.e. antenna positions) is 3, the maximum number of singular vectors which can be removed is 2.

B. Image Reconstruction Algorithm and Performance Metrics

The resulting images of the axillary region are reconstructed using a wave-migration algorithm [14] considering the frequency band 2 to 5 GHz. The algorithm considers only the subset $\mathbf{G_I}$ which provides better results: angular antenna position E to I and horizontal antenna position 3 to 6 (shown in Fig. 2). A spatial filter is applied to remove the artefacts from the breast and arm regions which are included in the phantom and may hamper the evaluation of the images.

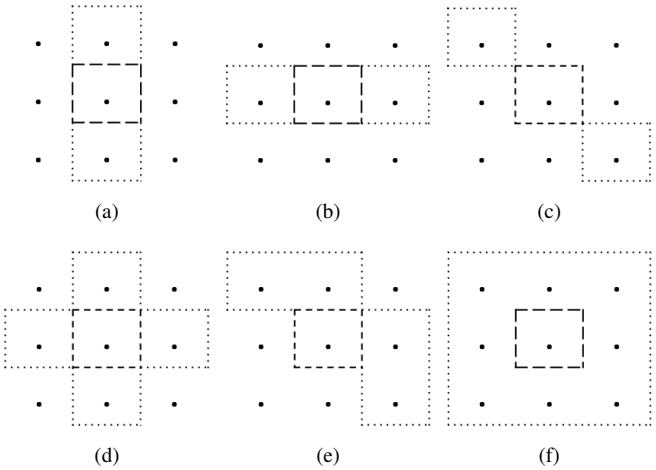

Fig. 4. Subsets of neighbouring antenna positions to perform factorisation of $\mathbf{s}_{a,h}$. The dashed line represents the (a, h) antenna position and the dotted line represents the neighbouring antenna positions.

The performance metrics used to evaluate the imaging results with the different parameters of SVD were Signal-to-Clutter Ratio (SCR) and Location Error (LE). SCR and LE are considered acceptable when they are higher than 1.5 dB and lower than ALN dimensions (i.e. 20 mm), respectively.

IV. Results and Discussion

Three experimental tests were conducted with ALNs in different positions: one in a central position between the breast and the arm (ALN-1), one close to the breast (ALN-2), and one close to the arm (ALN-3). Fig. 5 shows the performance metrics of imaging results of the three experimental tests considering the different subsets of neighbouring antenna positions over the number of singular vectors removed with SVD.

In all three tests, when considering Vertical 3, Horizontal 3 and Diagonal 3, either SCR is too low or LE is too high when only one or two singular vectors are removed. We verify that the number of singular vectors is not enough to successfully separate the air/dielectric response from the ALN response, and therefore ALN detection is not possible.

When considering the subsets Cross 5, Diagonal 5 and Block 9, the signals are decomposed in a higher number of singular vectors. As shown in Fig. 5, when three or more singular vectors are removed, the performance of the artefact removal improves. However, Diagonal 5 still presents a high LE for ALN-2. Both Cross 5 and Block 9 subsets present similar performance behaviour within the three experimental tests. When the number of singular vectors removed is higher than 5, Cross 5 cannot be used while the performance of Block 9 shows an increase of LE.

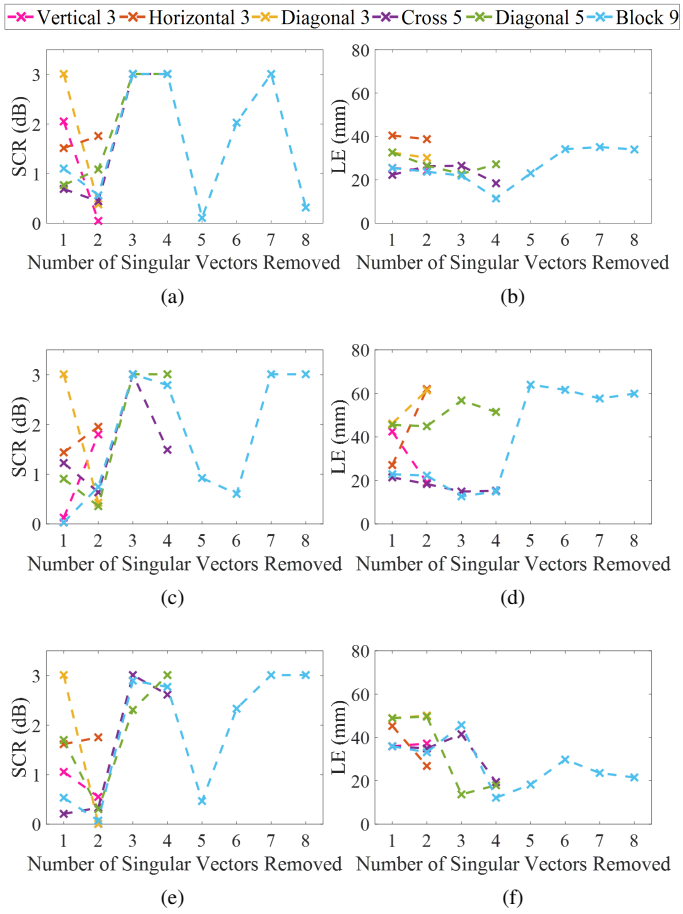

Fig. 5. Performance metrics over the number of singular vectors removed for each subset of neighbouring antenna positions and the three experimental tests. Signal-to-Clutter Ratio and Location Error are shown on the left and right columns, respectively. (a) and (b) correspond to imaging results of ALN-1, (c) and (d) to imaging results of ALN-2, and (e) and (f) to imaging results of ALN-3.

The minimum LE is obtained for ALN-1, ALN-2 and ALN-3 when four singular vectors are removed considering Block 9. LE is 11.4, 14.9 and 12.2 mm for ALN-1, ALN-2 and ALN-3, respectively. SCR is higher than 2.77 dB in all tests, well above the minimum 1.5 dB. There are two reasons which may explain why Block 9 with four removed singular vectors are the optimal combination. Firstly, the air/dielectric response is successfully separated from the ALN response when a high number of singular vectors is obtained with SVD. Lastly, when a higher number of antenna positions is considered for the SVD algorithm, the probability that the majority of the antenna positions record similar air/dielectric response is also higher, ultimately improving the factorisation performance.

V. Conclusion

In this paper, we studied the importance of the selection of antenna positions on the artefact removal procedure to improve imaging results of MWI applications when applied to irregular body shapes. In particular, we performed our study using a new MWI prototype to aid breast cancer staging through ALN detection.

We proposed a methodology which tests different subsets of antenna positions and parameters of the artefact removal algorithm to optimise the artefact removal and, consequently, the target detection. The best combination of parameters and subset of antenna positions is found by comparing the performance metrics of imaging results.

For the ALN-MWI application, we considered SVD as the artefact removal algorithm to remove the air/dielectric reflections and we addressed three experimental tests with an ALN in different positions. We observed that different subsets of antenna positions and different number of singular vectors removed provide distinct artefact removal performances. The best performance was obtained when four singular vectors were removed from the factorisation of each antenna position and the surrounding eight neighbouring antenna positions were used.

In the future, a detailed comparison with other artefact removal algorithms will be performed and presented to the community. The results presented on this paper will be validated with other anatomically realistic phantoms of the axillary region, with more complex scenarios and used to further develop our ALN-MWI prototype.

Acknowledgment

This work is supported by Fundação para a Ciência e a Tecnologia-FCT under the fellowship SFRH/BD/129230/2017, FCT/MEC (PIDDAC) under the Strategic Programme UIDB/00645/2020, and also in part by FEDER-PT2020 Partnership Agreement under Grant UIDB/EEA/50008/2020. This work is developed in the framework of COST Action CA17115 – MyWAVE.

The authors would like to thank António Almeida for his help with the setup creation and measurements, Dr. Durval Costa at Champalimaud Foundation for providing the CT image used to create the axillary phantom under protocol "MMWave" (17/10/2018), and Duarte Guerreiro for initial processing of the images so the axillary region model could be printed in 3D.

References

[1] American Joint Committee on Cancer, "Breast Cancer," in *AJCC Cancer Staging Manual*, 8th ed. Springer, 2018.

[2] H. Rahbar, S. C. Partridge, S. H. Javid, and C. D. Lehman, "Imaging Axillary Lymph Nodes in Patients with Newly Diagnosed Breast Cancer," *Current Problems in Diagnostic Radiology*, vol. 41, no. 5, pp. 149–158, 2012.

[3] R. Eleutério and R. C. Conceição, "Initial Study for Detection of Multiple Lymph Nodes in the Axillary Region Using Microwave Imaging," in *9^{th} European Conference on Antennas and Propagation (EuCAP)*, Lisbon, Portugal, 2015.

[4] D. M. Godinho *et al.*, "Extracting Dielectric Properties for MRI-based Phantoms for Axillary Microwave Imaging Device," in *14^{th} European Conference on Antennas and Propagation (EuCAP)*, Copenhagen, Denmark, 2020, doi:10.23919/EuCAP48036.2020.9135980.

[5] M. Savazzi *et al.*, "Development of an anthropomorphic phantom of the axillary region for microwave imaging assessment," *Sensors*, vol. 20, no. 17, pp. 1–20, 2020.

[6] A. W. Preece, I. Craddock, M. Shere, L. Jones, and H. L. Winton, "MARIA M4: clinical evaluation of a prototype ultrawideband radar scanner for breast cancer detection," *Journal of Medical Imaging*, vol. 3, no. 3, p. 033502, 2016.

[7] J. A. Vasquez *et al.*, "A Prototype Microwave System for 3D Brain Stroke Imaging," *Sensors*, vol. 20, no. 9, pp. 1–16, 2020.
[8] Champalimaud Foundation, "Champalimaud Foundation," 2020. [Online]. Available: http://first.fchampalimaud.org/en/
[9] J. M. Felício, C. A. Fernandes, and J. R. Costa, "Complex Permittivity and Anisotropy Measurement of 3D-Printed PLA at Microwaves and Millimeter-waves," in *22^{nd} International Conference on Applied Electromagnetics and Communications (ICECOM)*, Dubrovnik, Croatia, 2017, doi:10.1109/ICECom.2016.7843900.
[10] J. M. Felicio, J. M. Bioucas-Dias, J. R. Costa, and C. A. Fernandes, "Antenna Design and Near-Field Characterization for Medical Microwave Imaging Applications," *IEEE Transactions on Antennas and Propagation*, vol. 67, no. 7, pp. 4811–4824, 2019.
[11] N. Joachimowicz, C. Conessa, T. Henriksson, and B. Duchêne, "Breast Phantoms for Microwave Imaging," *IEEE Antennas and Wireless Propagation Letters*, vol. 13, pp. 1333–1336, 2014.
[12] J. W. Choi *et al.*, "Microwave detection of metastasized breast cancer cells in the lymph node; potential application for sentinel lymphadenectomy," *Breast Cancer Research and Treatment*, vol. 86, no. 2, pp. 107–115, 2004.
[13] T. R. Cameron, M. Okoniewski, and E. C. Fear, "A Preliminary Study of the Electrical Properties of Healthy and Diseased Lymph Nodes," in *International Symposium on Antenna Technology and Applied Electromagnetics & the American Electromagnetics Conference (ANTEM-AMEREM)*, Ottawa, ON, Canada, 2010, doi:10.1109/ANTEM.2010.5552566.
[14] J. M. Felício, J. M. Bioucas-Dias, J. R. Costa, and C. A. Fernandes, "Microwave Breast Imaging using a Dry Setup," *IEEE Transactions on Computational Imaging*, vol. 6, pp. 167–180, 2020.